

# Classical Toda lattice with domain wall initial conditions

Christian B. Mendl<sup>1</sup> and Herbert Spohn<sup>2</sup>

<sup>1</sup>Department of Informatics and Institute for Advanced Study, Technical University of Munich, Boltzmannstraße 3, 85748 Garching, Germany; christian.mendl@tum.de

<sup>2</sup>Department of Mathematics and Department of Physics, Technical University of Munich, Boltzmannstraße 3, 85748 Garching, Germany; spohn@tum.de

October 25, 2021

## Abstract

We study the classical Toda lattice with domain wall initial conditions, for which left and right half lattice are in thermal equilibrium but with distinct parameters of pressure, mean velocity, and temperature. In the hydrodynamic regime the respective spacetime profiles scale ballistically. For a particular range of parameters one observes a huge peak in the particle density. We study this phenomenon on the basis of generalized hydrodynamics. While the density diverges as  $1/|x|$ , with a different choice of coordinates smooth behavior is recovered.

## 1 Introduction

Over the past decade the out-of-equilibrium dynamics of many-body systems in one dimension has received a lot of attention, see for example the recent survey article [1]. Besides the laws governing the dynamics, also the initial conditions have to be specified. One popular choice is quantum quench [2,3], for which one prepares the ground (or thermal) state for a particular hamiltonian and then evolves in time according to some other translation invariant hamiltonian. A further much studied choice, the one discussed in our contribution, is domain wall: In the left/right half lattice one prepares thermal states of a given translation invariant hamiltonian. The product coupling of these states evolves then under the full hamiltonian. If in either half the thermodynamic parameters are identical, one deals with a small perturbation of a global equilibrium state. But if the parameters differ the time evolution is far from equilibrium. Besides being a physically natural choice, macroscopic properties can be predicted on the basis of a suitable hydrodynamic theory. Thus the comparison between analytical results and molecular dynamics simulations is in reach.

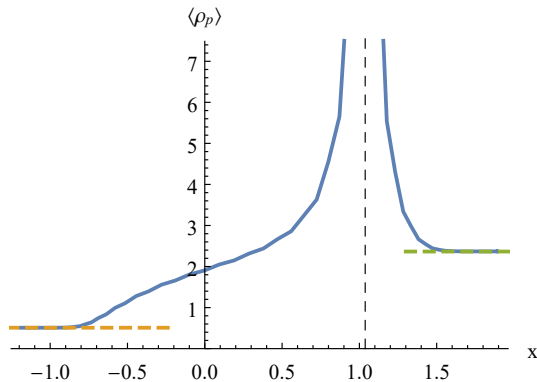


Figure 1: Average particle density as function of  $x$  at time  $t = 1$  for an initial domain-wall, left pressure  $P_- = \frac{1}{2}$  and right pressure  $P_+ = 2$  at uniform inverse temperature  $\beta = 1$ .

In our contribution we focus on the classical Toda fluid with initial domain wall. The dynamics is integrable and, in principle, generalized hydrodynamics (GHD) can be used for quantitatively predicting the ballistic spreading [4, 5]. Such numerical solutions of GHD have been reported in [19], including low order quantum corrections. As parameters the authors considered a uniform chemical potential and a jump in the temperature, corresponding to a left pressure  $P_- = 0.35$  and a right pressure  $P_+ = 0.13$ . The solution scales ballistically and, at some given time, the particle density drops spatially from 0.19 to 0.13 with a slight dip in the middle. Using a similar numerical scheme, in our GHD simulation we considered  $P_- = \frac{1}{2}$  and  $P_+ = 2$  at a uniform temperature. To our surprise, the particle density profile exhibits a  $1/|x|$  type singularity, compare with Fig. 1. The goal of our contribution is a more detailed understanding of how such a singularity arises.

Already in the pioneering contributions [4, 5] it was realized that the solution of the GHD domain wall problem has a very specific structure. In the  $x$ -(spectral parameter) plane one has to determine the contact line at which the spectral parameter jumps from its left to its right value. This contact line fully characterizes the solution, which brings us to a second motivation for our study. While the self-similar solution of generalized hydrodynamics is computed numerically, most commonly only plots for the spatial dependence of density, momentum, and temperature are displayed. We regard the contact line as more informative than low order moments and will numerically determine its shape.

To give an outline: We briefly discuss the domain wall solution for nonintegrable chains and for integrable, but noninteracting ones. Generalized hydrodynamics of the Toda lattice is recalled. We provide novel details of the solution behavior of the corresponding TBA equation. In the second part of our article we discuss the solution with domain wall initial conditions, thereby providing numerical data for the contact line and elucidating the origin of the singularity.

## 2 Domain wall for nonintegrable and noninteracting chains

We briefly recall the domain wall problem of conventional hydrodynamics, so to provide a contrast with integrable chains. Furthermore, to foreshadow the structure underlying GHD, the harmonic chain is used as a simplistic illustration of integrable chains.

We start by considering a wave field over  $\mathbb{Z}$ , displacements denoted by  $\{q_j \in \mathbb{R}, j \in \mathbb{Z}\}$ , which is governed by

$$\ddot{q}_j(t) = U'(q_{j+1}(t) - q_j(t)) - U'(q_j(t) - q_{j-1}(t)). \quad (2.1)$$

Here  $U$  is a smooth function, bounded from below and at least a one-sided linear growth at infinity. Note that the right side depends only on the increments of  $q$ . Physically one thinks of nonlinear springs coupling neighboring displacements,  $U$  is the corresponding potential and  $-U'$  the force. The dynamics is hamiltonian and derived from

$$H = \sum_{j \in \mathbb{Z}} \left( \frac{1}{2} p_j^2 + U(q_{j+1} - q_j) \right), \quad (2.2)$$

$q_j, p_j$  position and momentum of the  $j$ -th particle. For the harmonic potential, i.e.,  $U(x) = \frac{1}{2}x^2$ , Eq. (2.1) becomes the standard discrete linear wave equation. For a non-linear force, rather naively one would expect the dynamics to become chaotic. But based on the Kolmogorov-Arnold-Moser (KAM) theorem a mixed phase space, partially chaotic and partially quasi-periodic, is the more likely scenario. On the other hand, the domain wall setting is concerned with the infinite lattice, and how much of the KAM structure persists is a poorly understood subject. We proceed here with a scheme which seems to work in practice.

It will be convenient to first introduce the increments

$$r_j = q_{j+1} - q_j, \quad (2.3)$$

more physically referred to as stretch, which can have either sign. Clearly,  $H$  is the sum of translates of single site terms,

$$H = \sum_{j \in \mathbb{Z}} e_j, \quad e_j = \frac{1}{2} p_j^2 + U(r_j), \quad (2.4)$$

with  $e_j$  the translate of  $e_0$  to lattice site  $j$ .  $e_0$  is a smooth function of its arguments. The equations of motion (2.1) then turn into

$$\dot{r}_j = p_{j+1} - p_j, \quad \dot{p}_j = U'(r_j) - U'(r_{j-1}). \quad (2.5)$$

From the dynamics one reads off three local conservation laws, namely stretch, momentum and energy,

$$(r_j, p_j, e_j) \quad (2.6)$$

and their currents

$$(-p_j, -U'(r_{j-1}), -p_j U'(r_{j-1})). \quad (2.7)$$

While this derivation is straightforward, in principle there could be some other smooth function  $g_0$ , its translate to site  $j$  denoted by  $g_j$ , which is strictly local in the sense to depend only on finitely many  $r_j$ 's and  $p_j$ 's and moreover satisfies the discrete conservation law

$$\frac{d}{dt}g_j = \mathcal{J}_j - \mathcal{J}_{j+1}. \quad (2.8)$$

If such a current function  $\mathcal{J}_j$  exists at all, it has to be smooth and strictly local. As obvious from (2.8), the time change of  $\sum_{j=m}^{j=m'} g_j$  is then only through the boundary of the interval  $[m, \dots, m']$ . As an outstanding puzzle of the subject, a strict dichotomy seems to be valid. The nonlinear wave equation (2.1) has either three or a countably infinite number of conservation laws, the former case being called nonintegrable. Integrable chains are exceptional. The obvious candidate is the harmonic chain,  $U(x) = \frac{1}{2}x^2$ , see for example the discussion in [10]. Since the equations of motion are linear, the superposition principle holds. Thus, beyond being integrable the harmonic chain is also noninteracting. The respective GHD is a system of uncoupled conservation laws. The Toda chain, to be discussed below, is also integrable. But now GHD is a nonlinear system of coupled conservation laws, reflecting that the conserved fields interact.

To construct an initial domain wall state for a nonintegrable chain, note that the dual thermodynamic parameters are  $(P, \mathbf{u}, \beta)$ , pressure, mean velocity, and inverse temperature. Since  $H$  of (2.4) is a sum of one-point functions, in thermal equilibrium the  $\{r_j, p_j\}$ 's are independent and identically distributed with single site probability density function

$$\mu_{P, \mathbf{u}, \beta}(r_0, p_0) = Z(P, \mathbf{u}, \beta)^{-1} \exp \left[ -\beta \left( \frac{1}{2}(p_0 - \mathbf{u})^2 + U(r_0) + Pr_0 \right) \right], \quad (2.9)$$

$Z$  the normalizing partition function and  $P > 0$ ,  $\beta > 0$ . The thermal state does not change under the dynamics (2.5). For a domain wall state we prescribe left and right parameters,  $(P_{\pm}, \mathbf{u}_{\pm}, \beta_{\pm})$ . The  $(r, p)$ 's are still independent, but for  $j < 0$  we choose the parameter set  $(P_-, \mathbf{u}_-, \beta_-)$  and for  $j \geq 0$  the parameter set  $(P_+, \mathbf{u}_+, \beta_+)$ .

One would expect that on a macroscopic scale the state can be well characterized by block averaged values of the conserved fields. Given these values, the local distribution is close to the corresponding equilibrium state. Assuming such local equilibrium, one arrives at the coupled set of hydrodynamic equations

$$\partial_t \mathbf{l} + \partial_x \mathbf{j}_l = 0, \quad \partial_t \mathbf{u} + \partial_x \mathbf{j}_u = 0, \quad \partial_t \boldsymbol{\epsilon} + \partial_x \mathbf{j}_\epsilon = 0, \quad (2.10)$$

where the hydrodynamic currents are given by

$$(\mathbf{j}_l, \mathbf{j}_u, \mathbf{j}_\epsilon) = \left( -\mathbf{u}, P(\mathbf{l}, \boldsymbol{\epsilon} - \frac{1}{2}\mathbf{u}^2), \mathbf{u}P(\mathbf{l}, \boldsymbol{\epsilon} - \frac{1}{2}\mathbf{u}^2) \right). \quad (2.11)$$

Here  $\mathbf{l}(x, t)$ ,  $\mathbf{u}(x, t)$ ,  $\boldsymbol{\epsilon}(x, t)$  are the hydrodynamic fields of stretch, velocity, and total energy.  $P$  is the pressure depending on stretch and internal energy. From the microscopic model  $P$  is obtained by setting  $\mathbf{u} = 0$  in Eq. (2.9) and computing the averages  $\langle r_0 \rangle_{P, 0, \beta}$ ,  $\langle e_0 \rangle_{P, 0, \beta}$ . By inverting these functions one arrives at  $P$ . The Euler equations have to be solved with initial conditions

$$(\mathbf{l}(x, 0), \mathbf{u}(x, 0), \boldsymbol{\epsilon}(x, 0)) = \chi(\{x < 0\})(\mathbf{l}_-, \mathbf{u}_-, \boldsymbol{\epsilon}_-) + \chi(\{x \geq 0\})(\mathbf{l}_+, \mathbf{u}_+, \boldsymbol{\epsilon}_+). \quad (2.12)$$

Mathematically (2.10) – (2.12) are known as Riemann problem, extremely well studied in the context of a coupled set of hyperbolic conservation laws. For a very readable account we refer to [11]. Let us merely observe that the solution scales ballistically, i.e. depends on  $x, t$  only through the ratio  $x/t$ . The solution consists of spatial intervals either with constant profiles or smoothly varying profiles, the latter known as rarefaction waves. Possibly they are separated by jump discontinuities, called shocks. To our knowledge there are only a few studies which compare molecular dynamics of the chain with domain wall initial conditions to numerical solutions of the respective hydrodynamic equations. In [12, 13] the program is carried out for a hamiltonian with point hard core potential and alternating masses. Actually in this investigation the goal was to elucidate fluctuations of time-integrated currents, which are required as an input to establish a rarefaction wave. The to us most fascinating part of the study lies in observing how the microscopic motion manages to create and maintain a jump discontinuity.

The solution to the Riemann problem relies on properties of the Euler equation linearized at local equilibrium, in our case a  $3 \times 3$  matrix with matrix elements depending on the thermodynamic parameters. As the location  $x$  of the self-similar solution is varied, the corresponding thermodynamic parameters change and, in order to satisfy the boundary conditions, may be forced to switch between two branches characterized by distinct eigenvalues. In a rough sense, this is the mathematical mechanism behind the formation of shocks.

In the integrable case the linearized operator plays an equally important role. A particularly simple, but still instructive example is the chain with a harmonic interaction potential, for which the hydrodynamic equations read

$$\partial_t W(x, t; k) + \omega'(k) \partial_x W(x, t; k) = 0. \quad (2.13)$$

Our notation should indicate that the wave number  $k \in [-\pi, \pi]$  is the label of the conserved field, which itself depends on the space-time point  $(x, t)$ .  $\omega(k)$  is the dispersion relation, in our case  $\omega(k)^2 = 2(1 - \cos k)$ . But for more general harmonic couplings,  $\omega(k)^2$  would be a real analytic  $2\pi$ -periodic function with  $\omega(k)^2 \geq 0$ . The linearized operator is multiplication by  $\omega'(k)$  independent of  $x$ . As we will see, for the Toda lattice the corresponding operator is  $x$ -dependent, which makes it more difficult to construct a solution. In case of domain wall, the initial conditions for (2.13) read

$$W(x, 0; k) = \chi(\{x < 0\})W_-(k) + \chi(\{x \geq 0\})W_+(k). \quad (2.14)$$

Then the solution to (2.13), (2.14) is self-similar,  $W(x, t; k) = \mathbf{W}(x/t; k)$ , and

$$\mathbf{W}(\xi; k) = \chi(\{\xi < \tilde{\phi}(k)\})W_-(k) + \chi(\{\xi \geq \tilde{\phi}(k)\})W_+(k), \quad \tilde{\phi}(k) = \omega'(k). \quad (2.15)$$

For each  $k$  there is a unique contact point  $\tilde{\phi}(k)$ , at which the solution  $W(\xi; k)$  jumps from the left value to the right value. As an early prediction of GHD, all integrable models with initial domain wall admit a unique solution, which is of the form as in Eq. (2.15). Of course, the contact line,  $\tilde{\phi}$ , depends on the model. In the linear case  $\tilde{\phi}(k) = \omega'(k)$ , which is not invertible. For the Toda lattice  $\tilde{\phi}$  will be less explicit, but turns out to be invertible.

### 3 GHD of the Toda lattice

The Toda lattice is an anharmonic chain, for which the interaction potential is specified as  $U(x) = e^{-x}$ . Hence the hamiltonian is written as

$$H = \sum_{j \in \mathbb{Z}} \left( \frac{1}{2} p_j^2 + e^{-r_j} \right), \quad r_j = q_{j+1} - q_j. \quad (3.1)$$

In terms of the Flaschka variables [14]

$$a_j = e^{-r_j/2}, \quad b_j = p_j, \quad (3.2)$$

the Lax matrix is the tridiagonal real symmetric matrix with matrix elements

$$L_{j,j} = b_j, \quad L_{j,j+1} = L_{j+1,j} = a_j. \quad (3.3)$$

For the finite lattice  $[1, \dots, N]$  the  $N$  eigenvalues of  $L$  are conserved. As functions on phase space they are non-local [15], their local version being  $\text{tr}[L^m]$ ,  $m = 1, 2, \dots$  [14]. In generalized hydrodynamics such conserved fields are usually called charges or conserved charges and it is convenient to follow this practice. The locally conserved charges of the Toda lattice have a strictly local density given by

$$Q_j^{[m]} = (L^m)_{j,j}, \quad m = 1, 2, \dots, \quad (3.4)$$

with  $j \in \mathbb{Z}$ . In addition, the stretch is conserved with density

$$Q_j^{[0]} = r_j. \quad (3.5)$$

The respective current densities are of the form

$$J_j^{[0]} = -Q_j^{[1]}, \quad J_j^{[m]} = (L^m L^\downarrow)_{j,j}, \quad (3.6)$$

where  $L^\downarrow$  denotes the lower triangular part of  $L$ , see [16, 20]. By construction one arrives at the microscopic conservation laws

$$\frac{d}{dt} r_j = -p_j + p_{j+1}, \quad \frac{d}{dt} Q_j^{[m]} = J_j^{[m]} - J_{j+1}^{[m]}, \quad m = 1, 2, \dots \quad (3.7)$$

Because of the extensive number of conserved charges, thermal equilibrium has to be extended to generalized Gibbs ensembles (GGE). Generalized hydrodynamics is then obtained by averaging (3.7) in a local GGE state. There is some freedom in the choice of coordinates. The most convenient one comes from the observation that the GGE expectation of  $Q^{[m]}$  is the  $m$ -th moment of the density of states (DOS) of the Lax matrix. Therefore, the natural hydrodynamic fields are the DOS of the Lax matrix and in addition the stretch,  $\nu$ , both depending on the macroscopic space-time point  $(x, t)$ , see [17–19] for more details. The standard notation for the DOS is  $\nu \rho_p(v)$ , with  $\rho_p$  the particle density. Then the generalized hydrodynamic equations are

$$\partial_t \nu - \partial_x q_1 = 0, \quad \partial_t (\nu \rho_p) + \partial_x ((v^{\text{eff}} - q_1) \rho_p) = 0. \quad (3.8)$$

Here  $q_1 = \nu \int_{\mathbb{R}} dw w \rho_p(w)$  is the average momentum. The definition of the effective velocity is more lengthy. One introduces the integral operator

$$T\psi(w) = 2 \int_{\mathbb{R}} dw' \log |w - w'| \psi(w'), \quad w \in \mathbb{R}, \quad (3.9)$$

resulting from the two-particle phase shift of the Toda lattice. Then, for given  $\rho_p$ , the effective velocity is the solution of the linear integral equation

$$v^{\text{eff}}(v) = v + (T\rho_p v^{\text{eff}})(v) - (T\rho_p(v))v^{\text{eff}}(v), \quad (3.10)$$

where  $\rho_p(v)$  is viewed as a multiplication operator.

Writing GHD in this way, the domain wall problem looks inaccessible. Surprisingly, as a general property of GHD, one can transform to normal modes in such a way that the quasi-linear operator is diagonal. This transformation is accomplished by

$$n(v) = \frac{\rho_p(v)}{1 + (T\rho_p)(v)} \quad (3.11)$$

and the resulting normal form of the hydrodynamic equations reads

$$\nu \partial_t n + (v^{\text{eff}} - q_1) \partial_x n = 0, \quad (3.12)$$

see [20] for a proof. Note that the two-system has merged into a single equation. The symbol  $n(v)$  denotes the number density in spectral parameter space. In [16, 20], for the same object the notation  $\rho_\mu$  is used.

Below we need some further notions from GHD. The dressing transformation of a general function  $\psi$  is given by

$$\psi^{\text{dr}} = \psi + Tn\psi^{\text{dr}}, \quad \psi^{\text{dr}} = (1 - Tn)^{-1} \psi. \quad (3.13)$$

One also uses the notation  $[w^m]^{\text{dr}}$  for the dressing of the  $m$ -th power of the linear function. Note that the dressing is relative to  $n$ . After a few algebraic transformations based on (3.10), (3.11) and (3.13), the thermodynamic quantities can be expressed in terms of  $n$ , which will be convenient for the domain wall problem discussed below. Specifically, one arrives at

$$\rho_p(v) = n(v)[1]^{\text{dr}}(v). \quad (3.14)$$

A seemingly more explicit formula for the effective velocity is

$$v^{\text{eff}}(v) = \frac{[w]^{\text{dr}}(v)}{[1]^{\text{dr}}(v)}. \quad (3.15)$$

In addition

$$\nu^{-1} = \int_{\mathbb{R}} dw \rho_p(w) = \int_{\mathbb{R}} dw n(w)[1]^{\text{dr}}(w) \quad \text{and} \quad q_1 = \nu \int_{\mathbb{R}} dw n(w)[w]^{\text{dr}}(w). \quad (3.16)$$

*Thermal states.* — As discussed in [16, 18, 21], for thermal states,  $n(v)$  is a solution of the thermodynamic Bethe ansatz (TBA) equation,

$$V(w) - \mu - (Tn)(w) + \log n(w) = 0, \quad (3.17)$$

with  $V(w) = \frac{1}{2}\beta w^2$ . The “chemical potential”  $\mu$  is a Lagrange multiplier which ensures normalization as

$$\int_{\mathbb{R}} dw n(w) = P. \quad (3.18)$$

$\mu$  depends on the thermodynamic parameters  $\beta$  and  $P$ , and turns out to be equal to the free energy  $F(\beta, P)$ , for which an explicit formula is available [16],

$$F(\beta, P) = \log \sqrt{\beta/(2\pi)} + P \log \beta - \log \Gamma(P), \quad (3.19)$$

with  $\Gamma$  the Gamma function. The thermally averaged stretch is then the derivative of the free energy with respect to the pressure,

$$\nu = \partial_P F(\beta, P) = \log \beta - \psi(P), \quad (3.20)$$

$\psi$  denoting the digamma function.

Fig. 2 visualizes these thermal functions.  $F(\beta, P)$  is a concave function, and assumes its maximum at some critical pressure  $P_c > 0$ . Thus the average stretch  $\nu$  decreases with increasing  $P$  and crosses zero at  $P_c$ . For small pressure particles are far apart and the density is low. As  $P$  is increased, the distance between neighboring particles shrinks and vanishes at  $P_c$ . Upon further increase the distance becomes negative. For  $P < P_c$ , positions are typically ordered as  $\dots < q_j < q_{j+1} < \dots$ , while for  $P > P_c$  order is reversed to  $\dots < q_{j+1} < q_j < \dots$ . At  $P_c$  the typical distance between particles is of order  $1/\sqrt{N}$ , and the Toda fluid density diverges. For thermal equilibrium such properties are confirmed by an explicit computation. From the shape of  $F(\beta, P)$  (and thus of  $\mu$ ) one concludes that, in general, a given  $\mu$  is associated with two different values of  $P$ . Likewise on the level of (3.17) this property is reflected by two-valued solutions having a low and high pressure branch which match at  $P_c$ . While  $\rho_p$  diverges as  $P \rightarrow P_c$ ,  $\nu\rho_p$  and  $n$  vary smoothly through  $P_c$ . Any GGE is expected to show the same behavior.

*Numerical method.* — For the simulations we solve TBA numerically via Newton iteration (Mathematica’s FINDROOT), together with the quasi-energy parameterization  $n(w) = e^{-\varepsilon(w)}$  to ensure  $n(w) > 0$ . In practice, this requires a good starting point, which we obtain via an associated Fokker-Planck equation [21]. As sketch of a derivation, first insert  $n(v) = P\rho_s(v)$  into (3.17), which gives

$$V(w) - \mu - P(T\rho_s)(w) + \log \rho_s(w) + \log P = 0. \quad (3.21)$$

Differentiating this equation with respect to  $w$  and then multiplying by  $\rho_s(w)$  results in

$$V'(w)\rho_s(w) - 2P \int_{\mathbb{R}} dv \frac{1}{w-v} \rho_s(v)\rho_s(w) + \rho_s'(w) = 0. \quad (3.22)$$



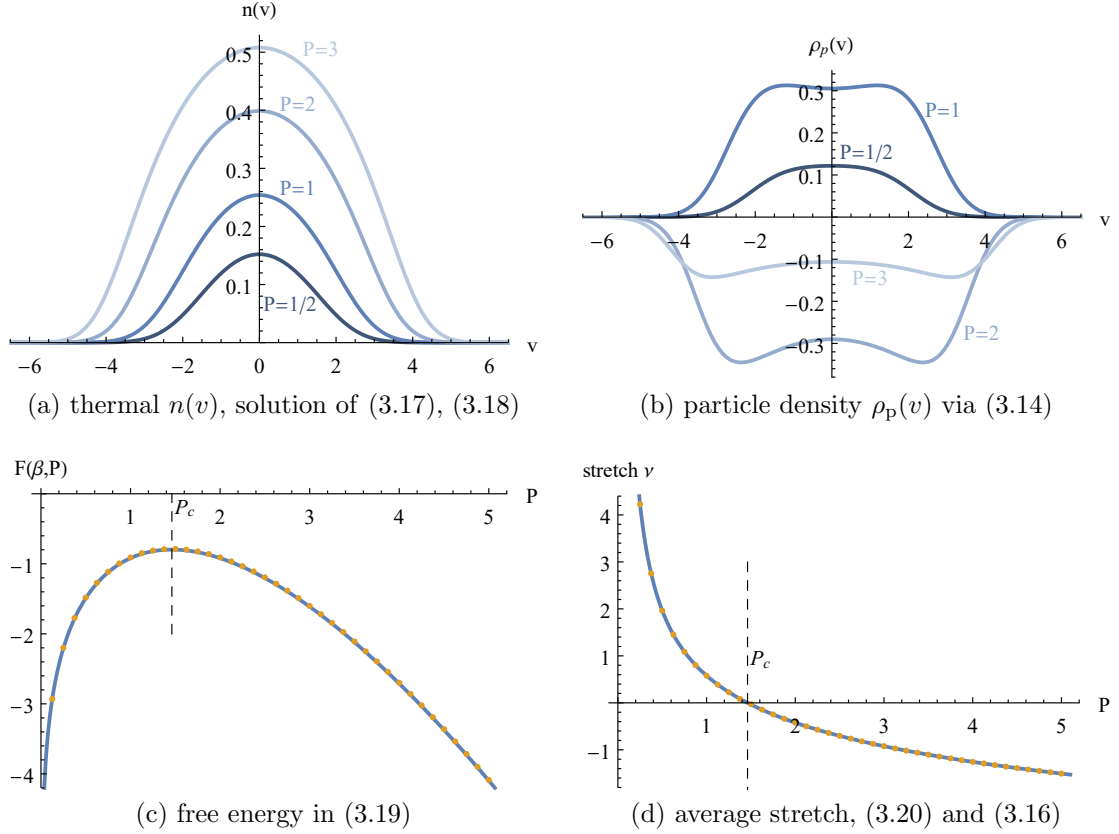


Figure 2: Thermal states for inverse temperature  $\beta = 1$ . (a)  $n(v)$  as obtained by solving the TBA equation (3.17) with normalization (3.18), for different values of  $P$ . (b) The corresponding particle density  $\rho_p(v)$  diverges at  $P_c$  and flips its overall sign as  $P$  crosses  $P_c$ . (c) Free energy (3.19), which coincides with the chemical potential  $\mu$  appearing in (3.17). As consistency check, the yellow dots show  $\mu$  obtained by inserting the Fokker-Planck stationary solution, (3.23), scaled by  $P$  into (3.17). (d) Average stretch: the solid line shows (3.20), and the yellow dots the stretch computed via (3.16)

$\rho_s$  can be interpreted as the stationary solution of the time-dependent nonlinear Fokker-Planck equation

$$\partial_t \rho(w, t) = \partial_w \left( V'(w) \rho(w, t) - 2P \int_{\mathbb{R}} dv \frac{1}{w-v} \rho(v, t) \rho(w, t) \right) + \partial_w^2 \rho(w, t). \quad (3.23)$$

Requiring the normalization  $\int_{\mathbb{R}} dw \rho_s(w) = 1$ , Eq. (3.23) has a unique stationary solution. While TBA and Fokker-Planck are equivalent analytically, we observed that, numerically, optimal precision is obtained by first solving the nonlinear Fokker-Planck equation, and then using these data as initial value for the TBA Newton iteration.

The integral transformation (3.9) has to be performed numerically as well. A finite element discretization of  $n(v)$ ,  $\rho_p(v)$ ,  $v^{\text{eff}}(v)$ , etc. via hat functions on a uniform grid works well in practice. Specifically, we use the grid spacing  $h = \frac{1}{10}$ .

The action of the integral operator (3.9) can be symbolically precomputed for these hat functions, and the discretization of  $T$  is a symmetric matrix. The dressing transformation (3.13) then amounts to solving a linear system of equations.

## 4 Solution to the domain wall initial condition

We slightly rewrite Eq. (3.12) as

$$\partial_t n(x, t; v) + \tilde{v}^{\text{eff}}(x, t; v) \partial_x n(x, t; v) = 0, \quad \tilde{v}^{\text{eff}}(v) = \nu^{-1}(v^{\text{eff}}(v) - q_1). \quad (4.1)$$

The domain wall initial conditions are

$$n(x, 0; v) = \chi(\{x < 0\})n_-(v) + \chi(\{x \geq 0\})n_+(v). \quad (4.2)$$

Instead of  $n_{\pm}$ , physically it might be more natural to prescribe the DOS of the Lax matrix and the average stretch. But mathematically the normal form (4.1) is more accessible.

Since the solution to (4.1), (4.2) scales ballistically, we set  $n(x, t; v) = \mathbf{n}(t^{-1}x; v)$  and  $\tilde{v}^{\text{eff}}(x, t; v) = \tilde{\mathbf{v}}^{\text{eff}}(t^{-1}x; v)$ . Without loss of generality one adopts  $t = 1$  and arrives at

$$(x - \tilde{\mathbf{v}}^{\text{eff}}(x; v)) \partial_x \mathbf{n}(x; v) = 0, \quad \lim_{x \rightarrow \pm\infty} \mathbf{n}(x; v) = n_{\pm}(v). \quad (4.3)$$

Therefore  $x \mapsto \mathbf{n}(x; v)$  for fixed  $v$  has to be constant except for jumps at the zeros of  $x \mapsto x - \tilde{\mathbf{v}}^{\text{eff}}(x; v)$ . At this stage, it is not clear at which level of generality to proceed. Physically, one would expect to have a unique solution. Thus in the  $(x, v)$ -plane there should be a *contact line* which divides the plane into two domains, one containing the set  $\{-\infty\} \times \mathbb{R}$  and the other the set  $\{\infty\} \times \mathbb{R}$ . The solution  $\mathbf{n}(x; v)$  equals  $n_{\pm}(v)$  on either domain with a jump across the contact line. From the example of the harmonic chain, one would expect to have a unique contact point for every  $v$ . Then the contact line is the graph of the function  $v \mapsto \tilde{\phi}(v)$ . In the case of hard rods [6],  $\tilde{\phi}$  is invertible, inverse denoted by  $\phi$ . Hence the contact line is the graph of  $x \mapsto \phi(x)$ . We write our argument for the latter case, since hard rods can be considered as a limiting case of the Toda lattice. A more general contact line could be handled in a similar fashion.

With our assumptions, for every  $x$  there is a contact point  $\phi(x)$ . Then the solution ansatz reads

$$n^{\phi}(v) = \chi(\{v > \phi\})n_-(v) + \chi(\{v \leq \phi\})n_+(v) \quad \text{and} \quad \mathbf{n}(x; v) = n^{\phi(x)}(v). \quad (4.4)$$

The superscript  $\phi$  will be used to generically indicate that in the TBA formalism  $n^{\phi}$  is substituted for  $n$  and similarly the subscript  $\pm$  signals the substitution of  $n_{\pm}$ . For example, compare with (3.13), (3.16),

$$\psi^{\text{dr}, \phi} = (1 - Tn^{\phi})^{-1} \psi, \quad (\nu_{\pm})^{-1} = \int_{\mathbb{R}} dw \rho_{\text{p}\pm}(w) = \int_{\mathbb{R}} dw n_{\pm}(w) [1]^{\text{dr}, \pm}(w). \quad (4.5)$$

We set

$$\tilde{\mathbf{v}}^{\text{eff}}(x; v) = \tilde{\mathbf{v}}^{\text{eff}, \phi(x)}(v). \quad (4.6)$$

Then the condition on the left side of (4.3) translates to

$$x = \tilde{\mathbf{v}}^{\text{eff}}(x, \phi(x)). \quad (4.7)$$

Put differently, one defines

$$G(\phi) = \tilde{\mathbf{v}}^{\text{eff}, \phi}(\phi), \quad (4.8)$$

then

$$x = G(\phi(x)), \quad \phi(x) = G^{-1}(x), \quad (4.9)$$

which means that  $G$  is the inverse of the contact line  $\phi$ .

While  $G(\phi)$  itself has to be obtained numerically, the large  $|\phi|$  asymptotics can still be argued analytically. We start from

$$v^{\text{eff}, \phi}(\phi)(1 + T\rho_p^\phi(\phi)) = \phi + (T\rho_p^\phi v^{\text{eff}, \phi})(\phi). \quad (4.10)$$

Setting

$$n^\phi(v) = n_+(v) + \chi(\{v > \phi\})(n_-(v) - n_+(v)), \quad (4.11)$$

we note that for large  $\phi$  the second term is exponentially small and can be neglected. The second summand on the left of (4.10) then reads

$$2 \int_{\mathbb{R}} dw \log |\phi - w| \rho_{p,+}(w) \simeq 2 \log \phi \int_{\mathbb{R}} dw \rho_{p,+}(w) = 2(\nu_+)^{-1} \log \phi. \quad (4.12)$$

Similarly for the right side of (4.10) one finds a logarithmic increase with a prefactor  $c_+$ , which could be determined by a further iteration. The term  $q_1^\phi/\nu^\phi$  converges to  $q_{1,+}/\nu_+$ . Thus for  $\phi \rightarrow \infty$  one arrives at

$$G(\phi) \simeq \frac{\phi + c_+ \log |\phi|}{\nu_+ + 2 \log |\phi|} - \frac{q_{1,+}}{\nu_+}. \quad (4.13)$$

For  $\phi \rightarrow -\infty$ , the same asymptotics holds upon substituting  $\nu_-, c_-$  for  $\nu_+, c_+$ . If the boundary terms  $n_\pm$  have exponential decay, the error in (4.13) would be of the same order.

*Exemplary numerical solution.* — To explore the singularity as shown in Fig. 1, we solve the domain wall problem using thermal states in the left and right half, characterized by a constant inverse temperature  $\beta = 1$  and pressures  $P_- = \frac{1}{2}$ ,  $P_+ = 2$ , respectively, such that  $P_- < P_c < P_+$ . The results are shown in Fig. 3. Starting from  $n^\phi(v)$  defined in (4.4), all the other hydrodynamic functions can be obtained via dressing transformations. While  $n^\phi(v)$  pointwise agrees with  $n_\pm(v)$  by construction, this is no longer the case for the normalized particle density  $\nu^\phi \rho_p^\phi(v)$  shown in Fig. 3b. For comparison, the dashed curves in Fig. 3 visualize the functions corresponding to thermal  $n_\pm(v)$ .

We note that the contact line passes smoothly and with a non-zero slope through the point for which  $\nu = 0$ , implying a  $1/|x|$  type singularity for the

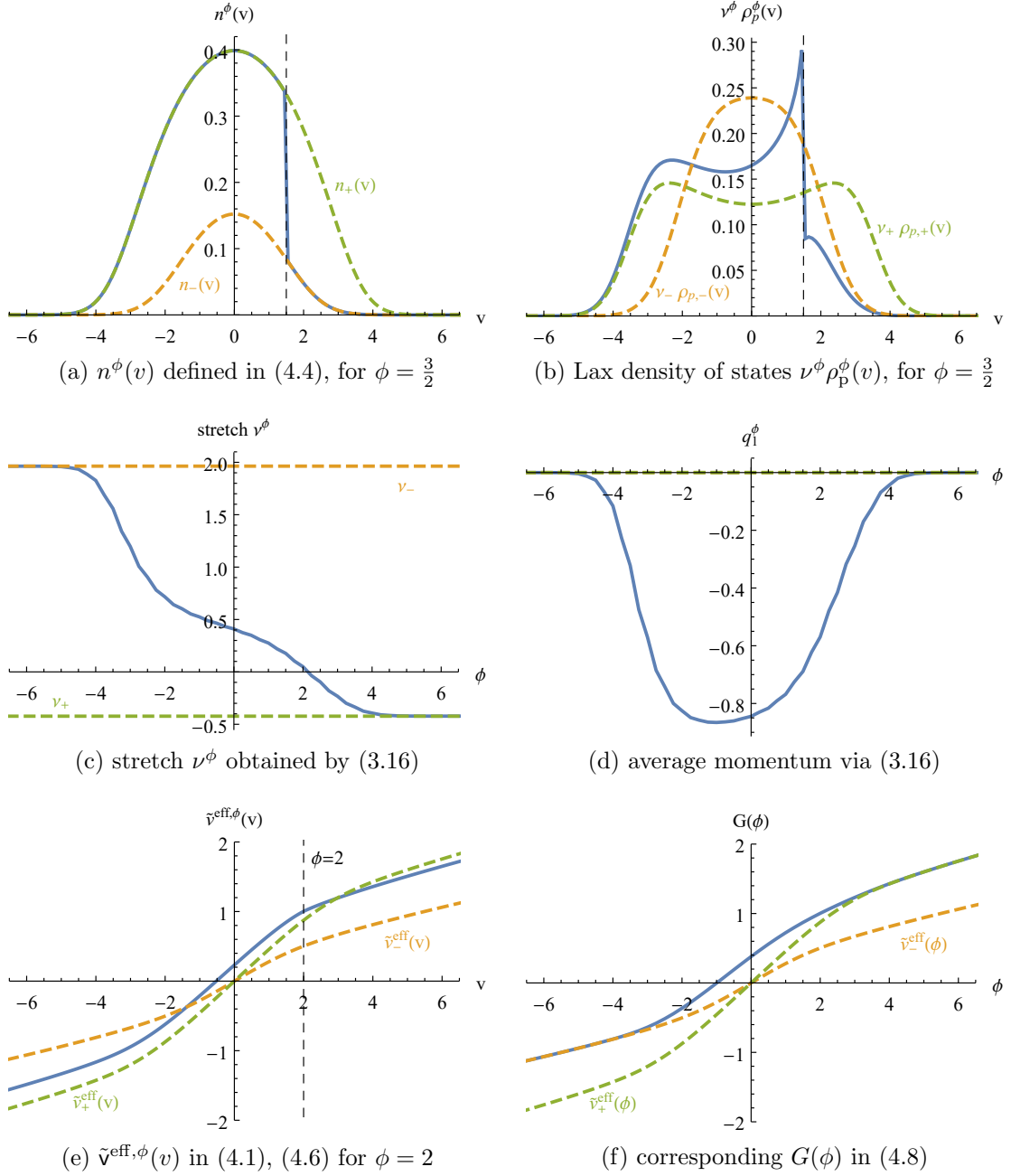


Figure 3: Numerical domain wall simulation results. The initial thermal states in the left and right domain (dashed curves) are specified by inverse temperature  $\beta = 1$  and pressure  $P_- = \frac{1}{2}$ ,  $P_+ = 2$ , respectively. Even though  $\nu^\phi$  crosses zero around  $\phi = 2$ , the rescaled effective velocity  $\tilde{\nu}^{\text{eff},\phi}$  remains finite.

particle density. On the other hand, the factor  $\nu^{-1}$  in the definition (4.1) of  $\tilde{v}^{\text{eff}}$  does not lead to a singular behavior. Of course, the density really diverges, but when viewed in a different coordinate system the behavior is smooth. We have tried various choices for the right/left parameters, and found that the contact line looks qualitatively similar in each case.

## 5 Conclusions and related work

On the Euler scale there is a sharp step at the contact line. One expects that, because of dissipation, the step is actually broadened to an error-like function. For the Toda lattice, and in general for integrable systems, the structure of diffusive corrections are available [22]. But numerical simulations of the Toda lattice are still missing. The broadening is convincingly observed in the XXZ model [23].

Domain wall initial conditions have been studied numerically for the discrete sinh-Gordon model [24]. Most detailed studies are available for the XXZ model [25,26]. In this case the spectral parameter space has in addition the type of string states and the contact line is upgraded to a contact sheet.

Because of momentum conservation the contact line of the Toda lattice is supported on the full real line. For XXZ, and other discrete models, one usually observes a light cone, i.e., the contact line is supported on an interval and the boundary values are maintained up to an edge. Then the behavior near the edge often shows intricate oscillatory decay, which has been elucidated in considerable detail [27,28].

The singularity reported in our contribution seems to be special for the Toda lattice.

**Acknowledgements.** CM acknowledges support from the Munich Center for Quantum Science and Technology. HS thanks Tomohiro Sasamoto for his generous hospitality at Tokyo Institute of Technology, where the initial work was accomplished, and Benjamin Doyon for teaching on domain walls.

## References

- [1] B. Bertini, F. Heidrich-Meisner, C. Karrasch, T. Prosen, R. Steinigeweg, and M. Znidaric, Finite-temperature transport in one-dimensional quantum lattice models, [arXiv:2003.03334](https://arxiv.org/abs/2003.03334).
- [2] A. Polkovnikov, K. Sengupta, A. Silva and M. Vengalattore, Colloquium: nonequilibrium dynamics of closed interacting quantum system, *Rev. Mod. Phys.* **83**, 863 (2011).
- [3] L. Vidmar and M. Rigol, Generalized Gibbs ensemble in integrable lattice models, *J. Stat. Mech.* **2016**, 064007 (2016).

- [4] O. A. Castro-Alvaredo, B. Doyon, and T. Yoshimura, Emergent hydrodynamics in integrable quantum systems out of equilibrium, *Phys. Rev. X* **6**, 041065 (2016).
- [5] B. Bertini, M. Collura, J. De Nardis, M. Fagotti, Transport in out-of-equilibrium *XXZ* chains: Exact profiles of charges and currents, *Phys. Rev. Lett.* **117**, 207201, (2016).
- [6] B. Doyon and H. Spohn, Dynamics of hard rods with initial domain wall state, *J. Stat. Mech.* **2017**, 073210 (2017).
- [7] V. B. Bulchandani, R. Vasseur, C. Karrasch, and J.E. Moore, Solvable hydrodynamics of quantum integrable systems, *Phys. Rev. Lett.* **119**, 220604 (2017).
- [8] D. Bernard and B. Doyon, Conformal field theory out of equilibrium: a review, *J. Stat. Mech.* **2016**, 064005 (2016)
- [9] R. Vasseur and J. E. Moore, Nonequilibrium quantum dynamics and transport: from integrability to many-body localization, *J. Stat. Mech.* **2016**, 064010 (2016).
- [10] H. Spohn and J. L. Lebowitz, Stationary non-equilibrium states of infinite harmonic systems, *Commun. Math. Phys.* **54**, 97 (1977).
- [11] A. Bressan, Hyperbolic conservation laws: An illustrated tutorial. In *Modelling and Optimisation of Flows on Networks*, Cetraro, Italy 2009, Lecture Notes in Mathematics 2062, Springer, 2013.
- [12] C. B. Mendl and H. Spohn, Searching for the Tracy-Widom distribution in nonequilibrium processes, *Phys. Rev. E* **93**, 060101(R) (2016).
- [13] C. B. Mendl and H. Spohn, Shocks, rarefaction waves, and current fluctuations for anharmonic chains, *J. Stat. Phys.* **166**, 841 – 875 (2017)
- [14] H. Flaschka, The Toda lattice. II. Existence of integrals, *Phys. Rev. B* **9**, 1924 – 1925 (1974).
- [15] M. Henon, Integrals of the Toda lattice, *Phys. Rev. B* **9**, 1921 – 1923 (1974).
- [16] H. Spohn, Generalized Gibbs ensembles of the classical Toda chain, *J. Stat. Phys.* **180**, 4 – 22 (2020).
- [17] B. Doyon, Generalised hydrodynamics of the classical Toda system, *J. Math. Phys.* **60**, 073302 (2019).
- [18] B. Doyon, Lecture Notes on Generalised Hydrodynamics, *SciPost Phys. Lect. Notes* **18** (2020)
- [19] V. B. Bulchandani, X. Cao, and J. Moore, Kinetic theory of quantum and classical Toda lattices, *J. Phys. A* **52**, 33LT01 (2019).

- [20] H. Spohn, Ballistic space-time correlators of the classical Toda lattice, *J. Phys. A: Math. Theor.* **53**, 265004 (2020).
- [21] X. Cao, V. B. Bulchandani, and H. Spohn, The GGE averaged currents of the classical Toda chain, *J. Phys. A: Math. Theor.* **52**, 495003 (2019).
- [22] J. De Nardis, D. Bernard, and B. Doyon, Diffusion in generalized hydrodynamics and quasiparticle scattering, *SciPost Phys.* **6**, 049 (2019).
- [23] J. De Nardis, D. Bernard, and B. Doyon, Hydrodynamic diffusion in integrable systems, *Phys. Rev. Lett.* **121**, 160603 (2018).
- [24] A. Bastianello, B. Doyon, G. Watts, and T. Yoshimura, Generalized hydrodynamics of classical integrable field theory: the sinh-Gordon model, *SciPost Phys.* **4**, 045 (2018).
- [25] L. Piroli, J. De Nardis, M. Collura, B. Bertini, and M. Fagotti, Transport in out-of-equilibrium XXZ chains: Nonballistic behavior and correlation functions, *Phys. Rev. B* **96**, 115124 (2017).
- [26] G. Misguich, K. Mallick, and P.L. Krapivsky, Dynamics of the spin-Heisenberg chain initialized in a domain-wall state, *Phys. Rev. B* **96**, 195151 (2017).
- [27] M. Collura, A. De Luca, and J. Viti, Analytic solution of the domain-wall nonequilibrium stationary state, *Phys. Rev. B* **97**, 081111(R) (2018).
- [28] V. B. Bulchandani and C. Karrasch, Subdiffusive front scaling in interacting integrable models, *Phys. Rev. B* **99**, 121410(R) (2019).